JOURNAL OF CATALYSIS 66, 451–462 (1980)

Studies of the Nickel-Catalyzed Hydrogenation of Graphite

C. W. KEEP, S. TERRY, AND M. WELLS

Chemical Technology Division, AERE Harwell, Didcot, Oxfordshire, England

Received December 20, 1979; revised July 7, 1980

Controlled atmosphere electron microscopy has been used to study the effects of small nickel particles on the hydrogenation of single crystal graphite. These particles propagated channels in the graphite basal plane, the majority of these channels being parallel to the $\langle 11\bar{2}0 \rangle$ directions. Increase in channel propagation rate occurred with increase in temperature, but at temperatures above 1075 K nickel particle disappearance was frequent, believed to be due to diffusion of metal into the graphite structure. At higher temperatures graphite platelets were formed from immobile nickel particles. Quantitative analysis also revealed that the rate of carbon gasification was proportional to the external surface areas of individual particles and not to the leading catalyst/graphite interfacial area. All these effects and possible reaction mechanisms are discussed.

1. INTRODUCTION

The reactions between carbon and steam and carbon and hydrogen have been the subject of many investigations, most of which have emphasized the complex equilibria involved (*1*). In spite of its technological importance, however, very little information is available on the catalytic hydrogenation of carbon.

Tomita and Tamai (*2, 3*) have conducted several experiments to study the reactions with hydrogen of various metal-impregnated carbons at temperatures up to 1300 K. It was found that methane formation occurred in several stages with most metals and this was attributed to the different degrees of crystallinity of the carbons used. The order of catalytic effectiveness for various metals was $Rh \geq Ru \geq Ir > Pt > Ni \gg Pd \geq Co \geq Fe$.

Rewick *et al.* (*4*) have studied the platinum-catalyzed gasification, in hydrogen and water atmospheres, of three types of carbon. It was discovered that a maximum in the rate of methane production occurred at ~1125 K, and that the rate was proportional to (partial pressure of hydrogen)$^{1/2}$, suggesting that dissociation of hydrogen was occurring and was rate determining.

McKee (*5*) found that the graphite–hydrogen reaction was strongly catalyzed by iron, cobalt, and nickel, but that copper, zinc, lead, and silver, all of which are very potent catalysts for graphite oxidation, were inactive.

Tomita and Tomai (*6*) have also used optical microscopy techniques to investigate the qualitative catalytic behavior of several metals, including nickel, on the hydrogenation of graphite. The actual particles observed were about 1 μm, or even larger, in diameter, and cut channels in the graphite basal plane. The results suggested that, in general, the larger the catalytic particle, the faster its channel propagation rate.

Workers using controlled atmosphere electron microscopy (*7*) (CAEM) to study the catalysis of graphite oxidation by several metals (*8, 9*) (with particles of usually 2 to 200 nm in size) found that channel propagation rates were inversely proportional to particle size. This means that the amount of carbon gasified was independent of the size of the catalytic particles and suggests differences in the rate-determining step in oxygen and hydrogen, if a comparison can be made between the two particle size ranges investigated in the two techniques. CAEM has therefore been used either to confirm or refute these differences observed for

0021-9517/80/120451-12$02.00/0

nickel, and also to attempt to gain further insight into the mechanism of this reaction, by an *in situ* study of the catalyzed gasification of graphite in hydrogen.

2. EXPERIMENTAL

2.1. Technique

The controlled-atmosphere electron microscope, described in detail elsewhere (*7*), consists of a JEOL JEM 7A transmission electron microscope (up to 100 keV), into which a gas reaction cell can be inserted. A specimen, mounted on a platinum heater ribbon and incorporated into the gas reaction cell, can be continuously observed at temperatures up to 1500 K in various gas atmospheres. A recent development enables the specimen temperature to be estimated by *in situ* optical pyrometry, without any undue disturbance to the system (*10*). The transmission image is relayed to a closed circuit television system, and can be recorded on videotape. Conventional micrographs can also be taken.

2.2 Materials and procedure

The hydrogen used (BOC Ltd) was ~99% pure and was further purified by passing through a commercially available catalytic purifier, reducing the oxygen content to <0.1 vpm, and then through a 5A molecular sieve to remove water.

Naturally occurring single-crystal graphite from Ticonderoga, New York, was used. The crystals were purified using a method described previously (*11*) and cleaved using a standard technique (*12*) until optically transparent. These specimens were then mounted on platinum heaters and coated with approximately one monolayer of spectrographically pure nickel by vacuum evaporation from a heated tungsten filament. After mounting the heater in the cell and inserting the latter in the microscope, hydrogen was introduced at a pressure of 0.5 to 1 Torr, and allowed to flow over the specimen for half an hour before the start of the experiment. The specimen temperature was then increased gradually and any changes in the specimen image recorded for analysis later.

3. ANALYSIS

The video record could be transferred to 16-mm film for quantitative analysis, but in most cases this was unnecessary due to the relatively slow channel propagation rates. The required information could be obtained by taking conventional plate photographs at suitable time intervals, with the specimen still at temperature.

In some cases the relative thicknesses of various areas of the graphite surface were determined by optical density measurements from these plates.

4. RESULTS

4.1. General Observations

When nickel-coated graphite specimens were heated in hydrogen, nucleation of the nickel film, into round particles 10–25 nm in diameter, occurred at between 825 and 925 K. This was occasionally preceded by fragmentation of the film and the formation of particles with a filamentary appearance, though these became round on further heating. As the temperature was raised, the particles grew larger, and, on reaching a temperature of approximately 975 K, those in contact with edges or steps in the graphite began to cut channels parallel to the basal plane. Individual channels were of uniform depth, but frequently not of uniform width, being narrow at the point of formation, but wider along their length, due to a gradual change in the width of the particle as it moved. No widening of channels due to uncatalyzed hydrogenation was ever observed and experiments with the beam on and off proved conclusively that the electron beam was not having any noticeable effect. The channels were 50–200 nm wide and usually very straight, with occasional 60° changes in direction. Virtually all channels were formed parallel to the $\langle 11\bar{2}0 \rangle$ directions. Most of the particles

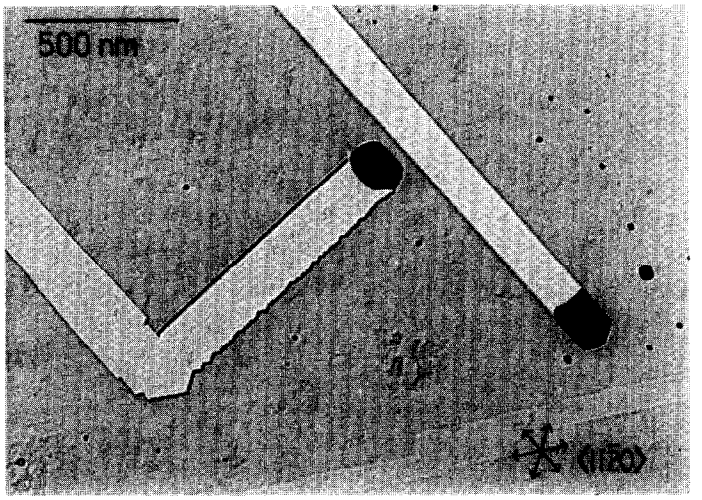

FIG. 1. Two nickel particles channelling in opposite crystallographic directions. Temperature 1025 K. Facets at the catalyst–graphite interface with both particles are in the $\langle 11\bar{2}0 \rangle$ directions.

were faceted at the leading graphite–catalyst interface, these facets also being oriented parallel to the $\langle 11\bar{2}0 \rangle$ directions, irrespective of the direction of the channel (see Fig. 1). Very occasionally, a particle was observed undergoing a 30 or 90° change in direction, indicating an actual change in crystallographic direction (see Fig. 1); its rate, however, appeared unchanged.

As the temperature was raised, the rate of channel propagation increased, until at temperatures above 1075 K (and occasionally at lower temperatures), the catalyst particles at the heads of some channels began to grow smaller, eventually disappearing altogether. This effect is shown in Fig. 3 when compared to Fig. 2, which shows the same group of channels before any nickel loss. This phenomenon occurred at different rates for different particles, and appeared to be independent of particle size, channel depth, and direction.

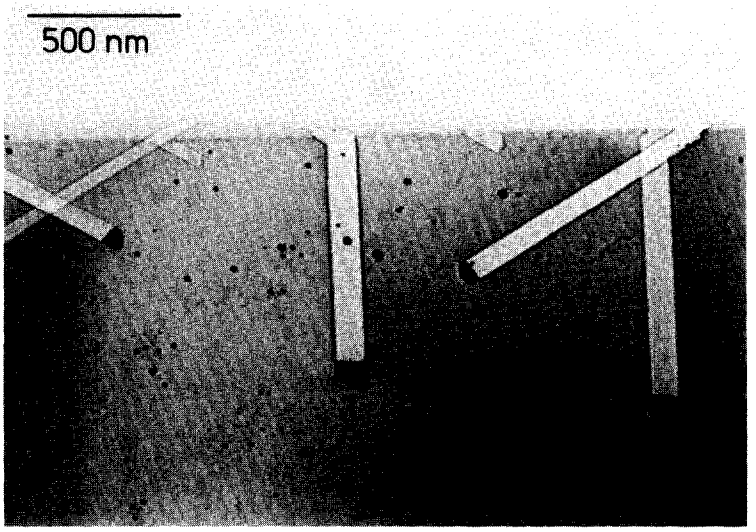

FIG. 2. Channelling nickel particles at 1075 K.

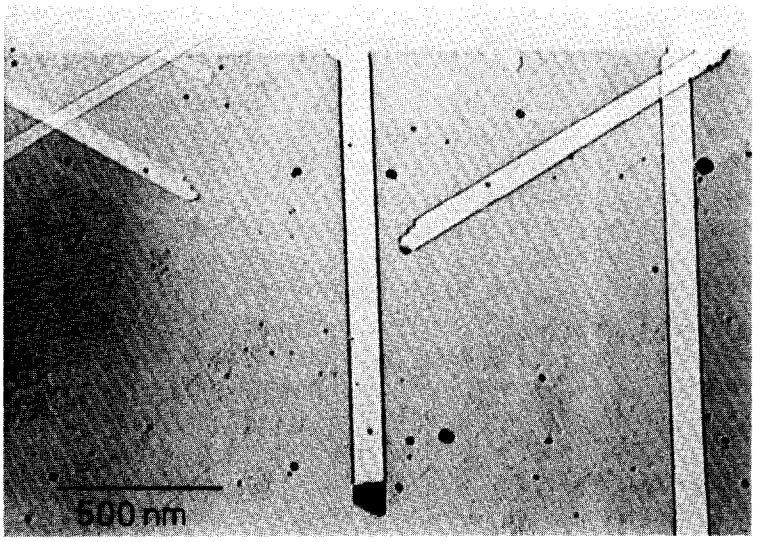

FIG. 3. Identical area to Fig. 2, showing loss of nickel from two of the channelling particles.

Particles which had not been channelling and were immobile on the surface were much more reluctant to disappear, and those which did so, at temperatures above 1175 K, left behind platelets of the same size and shape as the original metal particles (Figs. 4, 5, and 6 illustrate this phenomenon). When the specimen was heated in oxygen these platelets began to oxidize at the same temperature as the underlying graphite, suggesting that they are also graphitic in nature.

4.2. Quantitative Measurements

During the analysis of the results, quantitative measurements of various parameters involving channelling particles have been made, and in particular measurements of the rate at which channels are propagated. If these channels are linear, and do not

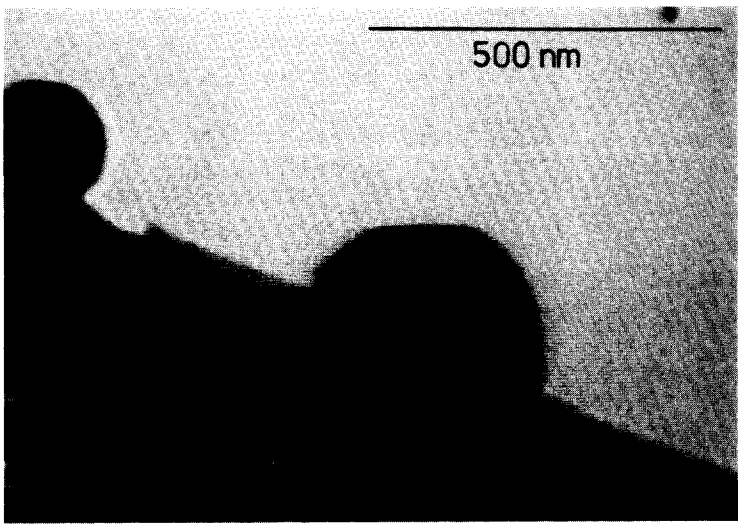

FIG. 4. Immobile nickel particles at 1150 K.

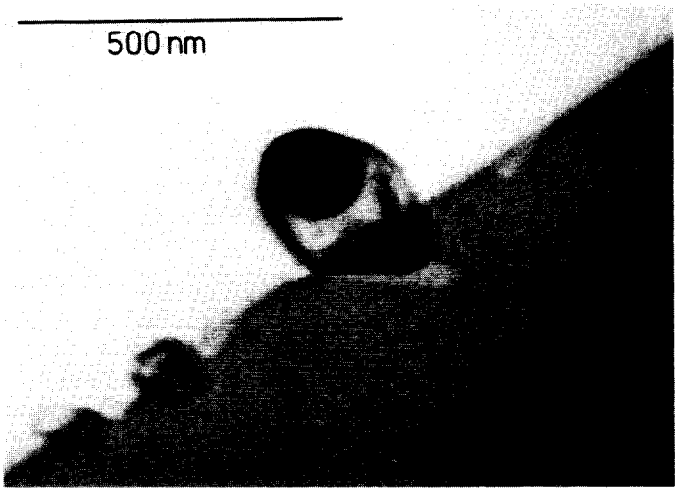

FIG. 5. Nickel disappearing from immobile particle at 1225 K.

change in width or depth, then the linear channel propagation rate is proportional to the rate of carbon gasification. If the channels are irregular, however, then the area of the channel produced by the particle (at constant depth) in unit time is more representative of the carbon gasification rate. In the analysis that follows, all of the channel propagation rates have been expressed as area of graphite removed per unit time.

Calculations have shown that there is less than 1 vpm of methane present in the gas phase as a direct result of formation by channelling particles. The rate data obtained will not therefore be restricted by gas phase equilibrium considerations at the temperatures used in this study.

Effect of temperature. Arrhenius plots of the channel propagation rate data obtained from individual particles yielded an apparent activation energy of 220 ± 40 kJ mol^{-1} over the temperature range 975 to 1050 K.

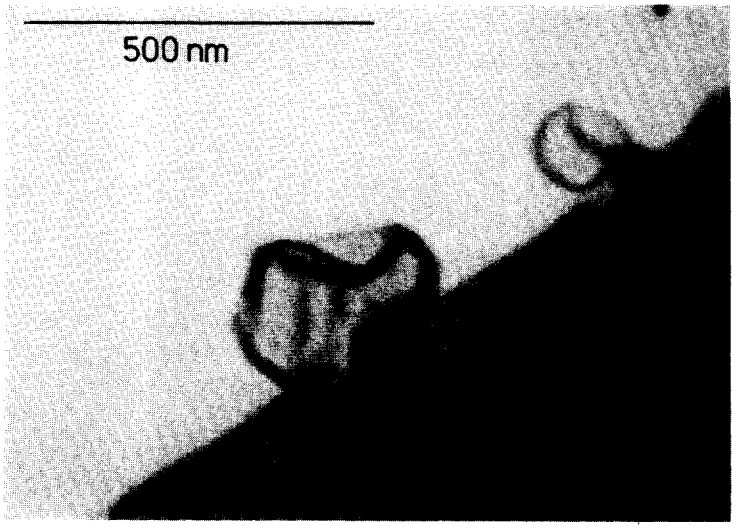

FIG. 6. Platelet remaining after complete nickel disappearance at 1225 K.

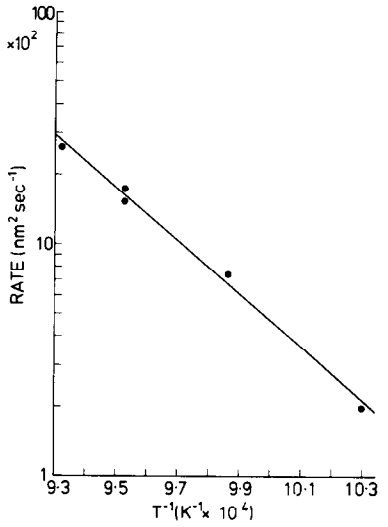

FIG. 7. Arrhenius plot for a particle propagating a channel of width 100 nm.

An example of a plot obtained from a 100-nm-wide particle propagating a straight channel is shown in Fig. 7.

Effects of particle size and channel depth. Occasionally, channelling particles underwent a gradual change in length, in some cases even becoming transparent to the electron beam (see Fig. 8). This increase in apparent area of the particle appeared to bring about an increase in channel propagation rate. Figure 9 confirms that, as a general rule, channel propagation rate was proportional to the apparent area of the catalyst particle, providing the particles compared were at the same temperature and cutting channels of equal depth. Exceptions to this rule occurred when the particles compared had different shapes, in which case comparison of apparent particle area would be misleading. To overcome this problem, specimens were shadowed with platinum–carbon in two directions at right angles, so that the heights and shapes of the particles could be estimated (*13*) and only those that were similar used for purposes of comparison. Particle shape varied from being flat (minimum detectable height 20 nm) to approximately hemispherical, the latter predominating.

No correlation was found between particle width and channel propagation rate for particles that were at the same temperature and cutting channels of equal depth, indicating that the area of the catalyst–graphite interface at the head of the channelling particle was not important in the rate determining process. The widths of the individual particles used to obtain the data

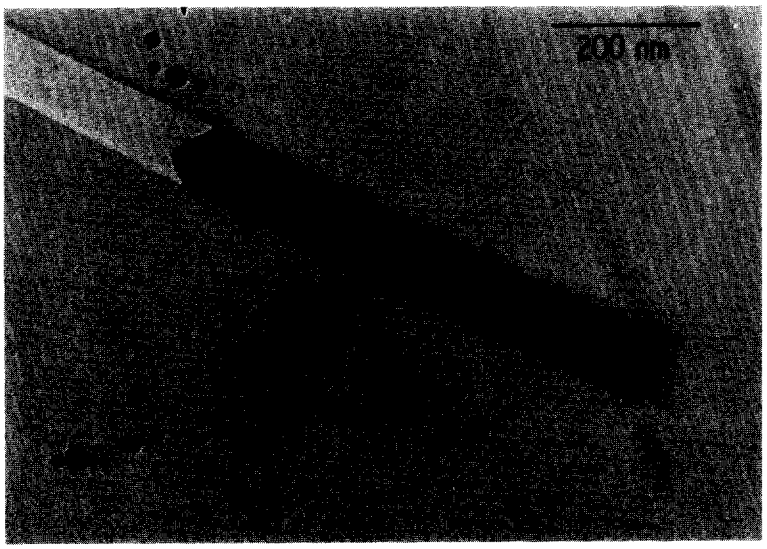

FIG. 8. Particle which had increased its length, and become transparent to the electron beam.

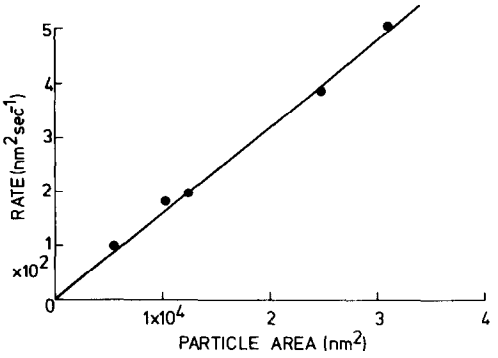

FIG. 9. Channel propagation rate versus apparent area of various particles channelling at the same depth in the graphite basal plane, at 1025 K.

for Fig. 9, for example, varied from 65 to 200 nm.

Table 1 shows the effect of channel depth (determined as a ratio by optical density measurements) upon the channel propagation rate. Comparison was made between pairs of particles at the same temperature and with similar areas. The results indicate that the channel propagation rate was inversely proportional to channel depth for particles of the same size; i.e., the *volume* of graphite gasified per unit time was independent of channel depth.

These effects of particle size and channel depth suggest that the only factor determining the amount of carbon gasified per unit time was the external surface area of the channelling particle. This was confirmed by comparing the rates of channel propagation by particles whose height, shape, and channel depth had been determined by shadowing. Absolute rates of carbon gasification (i.e., volume or amount of carbon gasified per unit time) could then be calculated, and compared with the true (calculated) surface areas of the individual particles. A comparison between various types of particle at 1035 K is shown in Table 2, and demonstrates that the ratio of carbon gasification rate to particle surface area remains constant at constant temperature.

5. DISCUSSION

5.1. Nickel Disappearance and Platelet Growth

The gradual disappearance of channelling particles can be explained by the occurrence of either of two processes. The metal could be evaporating from the surface or entering between the graphite layers. If the latter case were true it must be so dispersed as to be below the resolution of the instrument (2.5 nm). The phenomenon has been observed in other systems (*14–16*) involving different metals and different gases, suggesting that the presence of graphite is the crucial factor. In an attempt to resolve this problem, nickel was evaporated onto a silicon support and heated to 1200 K in hydrogen. Nucleation took place at 1000 K, but no decrease in particle size was observed upon increasing the temperature,

TABLE 1

Effect of Channel Depth upon Channel Propagation Rate for Particles A and B

Temperature (K)	Particle area ($nm^2 \times 10^4$)	Rate (nm^2sec^{-1})			Channel depth (ratio B/A)
		A	B	A/B	
975	3.3	18.5	15.1	1.25	1.30
1005	1.5	22.4	15.5	1.45	1.20
1005	1.5	89.0	22.4	4.0	4.40
1005	1.5	89.0	15.4	5.8	5.50
1025	1.8	175.8	95.0	1.85	2.40
1075	0.9	137.6	60	2.30	1.90

TABLE 2

Comparison of Carbon Gasification Rates Produced by Particles of Different Shape at 1035 K

Particle	Graphite area removed sec^{-1} (nm^2 sec^{-1})	Channel depth (nm)	Volume of graphite removed sec^{-1} (nm^3 $sec^{-1} \times 10^3$)	Apparent particle area ($nm^2 \times 10^4$)	Particle height (nm)	Calculated true particle surface area ($nm^2 \times 10^4$)	Volume gasification rate ÷ true surface area (nm $sec^{-1} \times 10^{-1}$)
A	520	5	2.6	1.86	<20	1.86	1.40
B	1020	10	10.2	3.06	120	7.05	1.45
C	550	5	2.75	1.37	40	1.96	1.40
D	468	10	4.68	1.51	80	3.31	1.41

suggesting that, in this system, nickel loss was not occurring.

Calculation of the vapor pressure of nickel particles (*17*) of the size predominating in the present study indicates that it will probably be only one to two orders of magnitude greater than for bulk material. Taking all these facts into consideration, it seems very likely that the cause of particle disappearance is diffusion of the metal into the graphite structure.

Another interesting phenomenon was the formation of graphite platelets from inactive nickel particles, when the temperature was raised above 1175 K. This suggests that, at this temperature, a substantial amount of carbon was dissolving in these inactive particles and being deposited when they gradually disappeared. Graphite has been formed by the dissolution–precipitation of carbon in cobalt and nickel (*18*), the process involving heating the metal in contact with amorphous carbon at 875 to 1275 K and then cooling rapidly, whereupon graphite was precipitated. Baker *et al.* (*19*) observed the precipitation of carbon from iron particles that had become immobile on graphite surfaces at 1175 K. Formation of carbon was not detected in the present study when the channelling particles disappeared, so there would appear to be less carbon present in channelling particles than in inactive ones, even though the ratio of the solubility of carbon in nickel at 1175 K (temperature above which platelets form) to that at 1075 K (temperature at which channelling nickel particles disappear) is only ~1.5 (*20*).

5.2. Effects of Particle Size and Channel Depth

It can be seen from Fig. 9 and Tables 1 and 2 that the amount of carbon gasified per unit time was proportional to the surface area of the channelling particle, and not to its width. This implies that reactions at the leading catalyst–graphite interface were not rate determining, in disagreement with suggestions by other workers (*6*), who also

found that in general the larger the catalytic particle, the faster its channelling rate.

In oxidation experiments using platinum (*8*), palladium (*8*), and molybdenum (*9*) as catalysts, it was found that the *linear* channel propagation rate was inversely proportional to particle size (expressed as particle width) for particles at the same temperature and channelling at similar depths, indicating that the overall carbon gasification rate was independent of particle size. This therefore is a major difference between hydrogenation and oxidation reactions.

5.3. Activation Energy

The apparent activation energy for the gasification of carbon by channelling nickel particles in hydrogen obtained in this study was 220 ± 40 kJ mol^{-1}, and was approximately constant over the temperature range used (975 to 1050 K). At higher temperatures rate data were difficult to obtain due to the frequent disappearance of the channelling particles. There have been no values reported recently for comparison with this result, except for a value of 110 ± 15 kJ mol^{-1} obtained by Tomita *et al.* (*3*) using a bulk, nickel-impregnated carbon sample, and values of 130 ± 12 kJ mol^{-1} (*21*), 140 ± 16 kJ mol^{-1} (in temperature range 775 to 875 K) (*22*), 265 ± 17 kJ mol^{-1} (at temperatures below 825 K) (*23*), and 180 ± 9 kJ mol^{-1} in temperature range 825 to 900 K (*23*) obtained from the hydrogenation of carbon deposited onto nickel from various hydrocarbons. The fact that these values fall roughly into two groups, one being approximately half the value of the other, suggests that perhaps the rate of reaction was controlled by diffusion in those experiments that resulted in the lowest activation energy (*1*).

Brennan and Fletcher (*24, 25*) have studied the rate of hydrogen atom production from the reaction of hydrogen with platinum, gold, and tungsten, finding apparent activation energies of 214 ± 5, 212 ± 7, and 217 ± 4 kJ mol^{-1}, respectively. If a similar value pertains to the production of hydrogen atoms from reactions with nickel, then this would suggest that hydrogen atom production might be the rate-determining step in the catalyzed hydrogenation of graphite.

The activation energies quoted above, however, have been determined by measuring the production of gaseous H atoms from the reaction of hydrogen with various metals and comparison with values obtained in this study can be made only if the rate-determining step in Brennan and Fletcher's experiments is some part of the chemisorption–surface dissociation process and not desorption of H atoms into the gas phase. The good agreement between the values for the activation energy might therefore be fortuitous.

5.4. Possible Reaction Mechanisms

The direction of the channelling particle is of particular interest, when attempting to elucidate the reaction mechanism. Virtually all the active particles in this study propagated channels in the $\langle 11\bar{2}0 \rangle$ direction. This reaction anisotropy has been observed in the past for the graphite–hydrogen system (*5, 6*) and also in the metal-catalyzed reaction of graphite with oxygen (*7, 9*) and carbon dioxide (*14*). This suggests that the removal of carbon atoms from the $(11\bar{2}l)$ face occurs more readily than from the $(10\bar{1}l)$ face (*26*). The fact that the facets at the graphite–catalyst interface were always oriented parallel to the $\langle 11\bar{2}0 \rangle$ directions, irrespective of channel direction, supports this view.

Tomita and Tamai (*6*) proposed a mechanism for the catalysis of graphite hydrogenation in which removal of carbon atoms from $(11\bar{2}l)$ faces was assumed to be fast, while removal of carbon from $(10\bar{1}l)$ faces was slow and rate determining. It can be seen from Fig. 9 and Tables 1 and 2, however, that the amount of carbon gasified per unit time was proportional to the surface area of the channelling particle and not to its width or channel depth. This suggests, therefore, that in the system studied here, "reaction" at the particle surface

was rate determining and not reaction at the graphite–catalyst interface. The rate of diffusion of active species to or from the interface does not appear to be the limiting step, since a dependence on particle radius, rather than area, would then be expected. Diffusion must, however, occur, and possible active species are hydrogen atoms (as hydrogen sorption is dissociative on nickel) (*27*) and carbon atoms, suggesting two possible types of reaction mechanism outlined below.

Mechanism A. It is suggested here that adsorption of hydrogen takes place onto the nickel particle surface, followed by dissociation into atoms. These atoms then diffuse (by bulk and/or surface processes) to the leading graphite–catalyst interface and react there to form methane. If the rate of reaction of these hydrogen atoms at the $(11\bar{2}l)$ face is greater than at the $(10\bar{1}l)$ face, then this will produce both the hexagonal facets at the leading particle–graphite interface and the preferred channel orientation. The rate-determining step is assumed to be some part of the chemisorption/dissociation process, as this would explain (a) the rate dependence upon the catalyst surface area, and (b) the rate independence on the leading catalyst–graphite interfacial area.

Other workers (*4, 28*) have suggested "spillover" of hydrogen atoms from metal surfaces as being the important process in the catalytic hydrogenation of graphite, but it has generally been assumed that the hydrogen atoms then migrate to active sites on the carbon surface, and react there to form methane. It may be postulated that methane is formed at the boundaries of the three phases carbon–hydrogen atom–nickel, i.e., at the head of the channelling particles.

Mechanism B. Another possibility involves an interaction between the catalyst and the graphite. Carbon dissolves in the nickel particle, diffuses through it to its outer surface where it reacts with hydrogen (gas phase, or sorbed) to form methane. This surface reaction would be rate-determining, in order to explain the observed effects of particle size. This mechanism has the advantage that there are no reactant and product pathway problems, as in mechanism A (*22*).

Recent studies (*29*) on the catalytic effect of nickel foils on the hydrogenation of carbon black and diamond in the temperature range 1173–1373 K have shown that solution of carbon occurred in the metal during the gasification process, lending support to this idea.

However, observations in support of mechanism A are:

(1) There appears to be more carbon present in inactive than in active nickel particles. If the gasification process proceeds by mechanism B, then the channelling particle would become saturated with carbon, as seems to be the case for inactive ones.

(2) The apparent activation energy obtained in this study for the gasification process is in very good agreement with values obtained for hydrogen atom production with several metals (but see Section 5.3).

(3) Long, "bullet-shaped" nickel particles (see Figs. 1 and 8) were observed quite frequently, demonstrating that reaction along the sides of these particles was negligible. It is difficult to understand why carbon solution should not occur if mechanism B prevails. If mechanism A is operative, however, either gaseous reactants or products might be causing the nickel particle not to "wet" the graphite along the channel sides. There might also be specific sites on the catalytic particle where gasification occurs, as has been suggested by other workers (*6*).

(4) Comparison between carbon and hydrogen permeabilities through nickel calculated from published data (*20, 30–34*) suggests that even the bulk hydrogen permeation rate alone (i.e., excluding any transport over the external surface of chan-

nelling particles) is approximately two orders of magnitude higher than that for carbon at 975 K.

These comparisons by themselves, however, do not prove that gasification is proceeding by mechanism A. For mechanism B to be feasible and consistent with the observed dependence of gasification rate upon particle surface area, carbon diffusion through channelling particles must be faster than the gasification rate at the surface of the particle enabling this surface reaction between carbon and hydrogen to be rate determining. This means then, if gasification occurs by mechanism B, that carbon must be capable of diffusing through particles of the size observed in this study (50–200 nm in width) at a rate that is faster than the gasification rate observed experimentally. The maximum rate of carbon diffusion occurs when this diffusional process is rate determining, i.e., when the concentration of carbon on the particle surface is zero. An approximate calculation of this rate of carbon diffusion is shown in the Appendix and demonstrates that gasification by mechanism B is possible.

A more definite conclusion as to the reaction mechanism may be reached when the catalytic effects of other metals in hydrogen and other gases have been completed (*14, 15*).

APPENDIX

Approximate Calculation of the Carbon Gasification Rate Expected if Carbon Diffusion through Nickel Catalyst Particles Is Rate Determining

Let us take the case of a "hemispherical" particle, channelling to a depth of 10 nm, the channel width and length being 100 nm, at a temperature of 1035 K. As can be seen from Table 2, at 1035 K the volume of carbon gasified per unit area of particle surface per second is 14×10^{-2} nm sec^{-1}. Therefore, the observed carbon gasification rate for this particle would be $2\pi \times 50^2 \times 14 \times 10^{-2}$ nm^3 of carbon sec^{-1}. The density of graphite is 2.25 g cm^{-3}, so that the observed gasification rate would be

$$2\pi \times 50^2 \times 14 \times 10^{-2} \times 10^{-21} \times 2.25 = 4.95 \times 10^{-18} \text{ g C sec}^{-1}.$$

If the reaction of carbon at the surface of the particle to form methane is fast compared with its rate of diffusion, then the surface concentration of carbon will be zero. Assume that the carbon concentration at the leading nickel–graphite interface is equal to its solubility at 1035 K (i.e., 9.52×10^{-3} g cm^{-3} (*20*)). The diffusion coefficient for carbon through nickel has also been determined (*20*) and is equal to 8.2×10^{-9} cm^2 sec^{-1} at 1035 K. The leading catalyst–graphite interfacial area = 10^{-11} cm^2.

The longest path length for carbon atoms diffusing through the particle will be 100 nm (i.e., from the leading graphite/catalyst interface to the rear of the particle). Therefore the rate of carbon diffusion through a "slab" of length 100 nm, using Fick's law in the steady state, will be

$$\frac{9.52 \times 10^{-3} \times 8.2 \times 10^{-9} \times 10^{-11}}{100 \times 10^{-7}} = 8.0 \times 10^{-17} \text{ g C sec}^{-1}.$$

This will obviously be an underestimate, as it neglects the radial diffusional flow of carbon to the outer hemispherical surface that will occur in the real situation; however, it can be seen that even the rate calculated above is faster than the experimental rate would be, showing that the catalyzed gasification of graphite by hydrogen could be occurring by diffusion of carbon atoms through nickel particles (i.e., by mechanism B).

REFERENCES

1. Walker, P. L., Rusinko, F., and Austin, L. G., *Adv. Catal.* **11**, 133 (1959).
2. Tomita, A., and Tamai, Y., *J. Catal.* **27**, 293 (1972).
3. Tomita, A., Sato, N., and Tamai, Y., *Carbon* **12**, 143 (1974).

4. Rewick, R. T., Wentrcek, P. R., and Wise, H., *Fuel* **53**, 274 (1974).
5. McKee, D. W., *Carbon* **12**, 453 (1974).
6. Tomita, A., and Tomai, Y., *J. Phys. Chem.* **78**, 22 (1974).
7. Baker, R. T. K., and Harris, P. S., *J. Sci. Inst.* **5**, 793 (1972).
8. Baker, R. T. K., France, J. A., Rouse, L., and Waite, R. J., *J. Catal.* **41**, 22 (1976).
9. Baker, R. T. K., Harris, P. S., Kemper, D. J., and Waite, R. J., *Carbon* **12**, 179 (1974).
10. Keep, C. W., Waite, R. J., and Terry, S., AERE Harwell report R9042 (1978); *J. Phys. E* **11**, 1002 (1978).
11. Keep, C. W., Waite, R. J., Terry, S., and Gadsby, G. R., AERE Harwell report M2780 (1976).
12. Hennig, G. R., *Chem. Phys. Carbon* **2**, 1 (1966).
13. Bradley, D. E., *in* "Techniques for Electron Microscopy" (D. H. Kay, Ed.), Chap. 3, p. 58. Blackwell Scientific Publications, Oxford, 1965.
14. Keep, C. W., Terry, S., and Waite, R. J., "Proc. Conf. on Gas Chemistry in Nuclear Reactors and Large Industrial Plant," held at Univ. Salford U.K., p. 196 (1980).
15. Keep, C. W., and Terry, S., Unpublished results.
16. Baker, R. T. K., Thomas, R. B., and Wells, M., *Carbon* **13**, 141 (1975).
17. Glasstone, S., "Textbook on Physical Chemistry," 2nd ed., Chap. VI, p. 495. Macmillan, New York, 1960.
18. Derbyshire, F. J., Presland, A. E. B., and Trimm, D. L., *Carbon* **13**, 111 (1975).
19. Baker, R. T. K., Feates, F. S., and Harris, P. S., *Carbon* **10**, 93 (1972).
20. Lander, J. L., Kern, H. E., and Beach, A. L., *J. Appl. Phys.* **23**, 12 (1952).
21. Figueiredo, J. L., and Trimm, D. L., *J. Catal.* **40**, 154 (1975).
22. Nishiyama, Y., and Tamai, Y., *Carbon* **14**, 13 (1976).
23. Bernardo, C. A., and Trimm, D. L., *Carbon* **17**, 115 (1979).
24. Brennan, D., and Fletcher, P. C., *Trans. Faraday Soc.* **56**, 1662 (1960).
25. Brennan, D., and Fletcher, P. C., *Proc. Roy. Soc. A* **250**, 389 (1959).
26. Thomas, J. M., *Chem. Phys. Carbon* **1**, 121 (1965).
27. Fast, J. D., "Interaction of Metals and Gases," Vol. 1, p. 123, Macmillan and Co. Ltd., London, 1965.
28. Robell, A. J., Ballou, E. V., and Boudart, M., *J. Phys. Chem.* **68**, 2748 (1964).
29. Grigor'ev, A. P., Lifshits, S. Kh., and Shamaev, P. P., *Kinet. Katal.* **18**(4), 948 (1977).
30. Smithells, C. J., and Ransley, C. E., *Proc. Roy. Soc. A* **155**, 195 (1936).
31. Lafitau, H., Gendrel, P., and Jacque, L., *Compt. Rend.* **263C**, 1033 (1966).
32. Schenck, V. H., Frohberh, M. G., and Jaspert, E. J., *Arch. Eisenhuettenw* **36**, 683 (1965).
33. Walker, B. F., Johnson, V. A., Hahn, W. C., and Wood, J. D., *Trans. AIME* **242**, 123 (1968).
34. See References in Stafford, S. W., and Mclellan, R. B., *Scripta Metal.* **9**, 1195 (1975).